



Article

Hydrogen Sorption and Rehydrogenation Properties of NaMgH₃

Luis Contreras ^{1,*}, Margarita Mayacela ¹ , Alberto Bustillos ² , Leonardo Rentería ³ and David Book ⁴

¹ Faculty of Civil and Mechanical Engineering, Research and Development Directorate, Technical University of Ambato, Ambato 180207, Ecuador; cm.mayacela@uta.edu.ec

² Faculty of Health Sciences, Medicine, Technical University of Ambato, Ambato 180207, Ecuador; aa.bustillos@uta.edu.ec

³ Faculty of Engineering, National University of Chimborazo, Av. Antonio José de Sucre, Riobamba 060108, Ecuador; leonardo.renteria@unach.edu.ec

⁴ School of Metallurgy and Materials, University of Birmingham, Edgbaston, Birmingham B15 2TT, UK; d.book@bham.ac.uk

* Correspondence: lf.contreras@uta.edu.ec; Tel.: +593-962795282

Abstract: The formation and hydrogen sorption properties of the NaMgH₃ perovskite/type hydride have been examined. Samples were mechanically ball milled under argon for 2, 5 and 15 h; then characterized by X-ray diffraction (XRD), differential scanning calorimetry (DSC), and thermogravimetric analysis (TGA) coupled with a mass spectrometer (MS). Lattice parameters and cell volume of the main NaMgH₃ phase increase as a function of milling. Dehydrogenation proceeded in two-step reactions for the NaMgH₃. The maximum amount of released hydrogen was achieved for the 2 h milled NaMgH₃ hydride accounting for 5.8 wt.% of H₂ from 287 °C to 408 °C. Decomposed NaMgH₃ samples were reversibly hydrogenated under 10 bar H₂ at ~200 °C.

Keywords: dehydrogenation; hydrogen storage; mechanical milling; perovskite hydrides; rehydrogenation



Citation: Contreras, L.; Mayacela, M.; Bustillos, A.; Rentería, L.; Book, D.

Hydrogen Sorption and Rehydrogenation Properties of NaMgH₃. *Metals* **2022**, *12*, 205. <https://doi.org/10.3390/met12020205>

Academic Editors: Roberto Figueiredo and Eric Mazzer

Received: 21 December 2021

Accepted: 17 January 2022

Published: 22 January 2022

Publisher's Note: MDPI stays neutral with regard to jurisdictional claims in published maps and institutional affiliations.



Copyright: © 2022 by the authors. Licensee MDPI, Basel, Switzerland. This article is an open access article distributed under the terms and conditions of the Creative Commons Attribution (CC BY) license (<https://creativecommons.org/licenses/by/4.0/>).

1. Introduction

Hydrogen has been extensively studied as a clean energy vector with the potential to replace carbon-based fuels. Nevertheless, to make it commercially available for mobile applications more efficient technologies for storage are demanded [1–6]. Solid-state storage provides attractive properties such as volumetric storage densities; however, the need to identify new materials with reversible characteristics, i.e., light-weight hydrides are needed [7–10].

Ternary hydrides have drawn special attention over the last decade; in particular Mg- base ternary hydrides are being extensively studied as potential storage materials for mobile applications, due to their light-weight, high gravimetric and volumetric capacity, abundance and low cost [11–14]. Extensive studies have demonstrated grain size reduction to a nanoscale enhances the kinetics and thermodynamics of hydrogen absorption and desorption properties [15,16]. However, more information is still required to fully understand the reactions and structural changes of these systems to consider them as candidates for on board vehicular energy storage applications.

Perovskite-type ternary hydrides with the structure ABH₃ (where H is the anion, A alkaline, alkali earth metal and B transition metal) are of special interest; mainly, magnesium and alkali elements given their relative abundance and light weight [17–19]. Moreover, it has been proven that replacing transition metal (B) with light metals (i.e., Li, Mg, Na) in the ABH₃ system can enhance gravimetric capacity [20,21] Fornari et al. studied the formation of MMgH₃ ternary hydrides, where (M = Na, K, Rb) [22]. It was found that KMgH₃ and RbMgH₃ decomposed an approximate of 3.5 wt.% of H₂ up to 400 °C. DFT computational studies reported in the literature, have predicted the possible formation of high-capacity hydrides LiMgH₃ (8.8 wt.% H₂) and Li₂MgH₄ (9.6 wt.% H₂). Nevertheless, these compounds have to be experimentally synthesized [11,19,22,23].

NaMgH₃ ternary hydride has stood out amongst the perovskite-type hydrides, due to its superior hydrogen mobility and high ionic conductivity which makes it a promising material for future electronic devices [24]. Moreover, due to its relatively high theoretical gravimetric and volumetric hydrogen storage properties (6 wt.%/88 kg/m³) [12,13], coupled with the ability to reversibly absorb and desorb H₂ under certain conditions of temperature and pressure, categorize this hydride as one of the most promising materials for mobile applications [25,26]. NaMgH₃ ternary hydride, presents an orthorhombic crystal structure similar to the GdFeO₃ type (Pnma space group) [27].

Sheppard et al. and Klaveness et al. described the desorption entropy ΔS (132.2 ± 1.3 kJ/mol H₂ K) and enthalpy ΔH (86.6 ± 1.0 kJ/mol H₂) of the NaMgH₃, showing improved thermodynamic stability in comparison to MgH₂ [28,29]. Nonetheless, dehydrogenation temperature at approximately 400 °C remains non appropriate to comply with the US DOE targets for on-board H₂ storage for light-duty vehicles [30]. Hence, obtaining lower dehydrogenation temperatures with enhanced thermodynamics of the NaMgH₃ perovskite-type hydride is required.

Wang et al. investigated the hydrogen sorption properties of the hydride and showed that thermodynamic properties of NaMgH₃ can be modified by adding new elements (alloys) and sorption kinetics can be enhanced by catalytic doping [31]. Hui Wu et al. [18] reported that due to the crystal chemistry structure of the NaMgH₃, it could be used for the formation of new compounds with enhanced hydrogen storage properties. Chaudhary et al. reported that by adding Si to NaMgH₃ decomposition temperatures can be lowered [32].

Numerous techniques for the formation of the NaMgH₃ ternary hydride have been described in the literature. For example, high-pressure H₂ sintering and cryo-milling [24,28,33] mechanochemical synthesis under Ar [20] and H₂ [14], and atmospheres. Mechanochemical techniques for synthesis were demonstrated to be advantageous in contrast to other techniques, not only because of the less energy intensive synthesis, but due to the grain size reduction which accelerates the H₂ desorption kinetics of the hydrides compared to those prepared at high temperature [26,34,35].

Ikeda et al. reported for the first time the formation ability of NaMgH₃ after mechanical milling NaH and MgH₂ under a hydrogen atmosphere, as well as the reversible hydriding and dehydriding reactions of NaMgH₃ [14,35]. Pottmaier et al. investigated the structure and thermodynamic properties of the hydride; it was shown that dehydrogenation occurs at 400 °C under 2 bar H₂ [24].

Recent studies, showed the facile synthesis of NaMgH₃ via reactive milling NaH and MgH₂ under Ar. It was found that after 5 h milling, single phase of NaMgH₃ ternary was formed with a maximum amount of hydrogen release equivalent to 4.7 wt.% [20]. Tao, S. et al. described the synthesis of NaMgH₃ + 5 wt.% g-C₃N₄ (NMH-5CN) composite by high-energy ball-milling, showing that the as milled material can desorb about 4.6 wt.% H₂ within 10 min at 365 °C suggesting that the incorporation of g-C₃N₄ improve the dehydrogenation properties of NaMgH₃ [26,36]. Hang, Z. et al. analyzed the enhancement of de/re-hydrogenation kinetics and cycling properties of NaMgH₃ by doping with lamellar-structure 2D carbon-based MXene, Ti₃C₂ demonstrating that with the introduction of 7 wt.% Ti₃C₂ it is possible to enhance the kinetic properties and lower the desorption temperature achieving a hydrogen desorption capacity of 4.8 wt.% of H₂ within 15 min at 365 °C [37].

Furthermore, rehydrogenation of perovskite-type NaMgH₃ has been reported in the various studies. For example, Ikeda et al. evidenced reversible formation of NaMgH₃ at 400 °C under 10 bar flowing H₂ from the decomposed phase of Na and Mg [35]. Hang, Z. et al. reported in his study, that lamellar-structure Ti₃C₂ can improve the reversibility of NaMgH₃, obtaining 4.6 wt.% H₂ capacity [37]. Nevertheless, the dehydrogenation temperatures offered by these compounds remain high and there is a need to find different ways to destabilize the ternary NaMgH₃ hydride. Recent studies by Zhang, X. et al. reported rehydrogenation of ultrafine MgH₂ nanoparticles (4–5 nm) and LiBH₄ nanocomposite achieving 6.7 wt.% H₂ capacity at 30 °C with a stable hydrogen cycling behavior in

50 cycles at 150 °C and 9.2 wt.% of H₂ at 300 °C with a stable cyclability up to 100 cycles, respectively [38,39]. Moreover, Ren, Z. et al. showed a reversible hydrogen capacity of 5 wt.% at 30 °C under 100 atm H₂ using sodium alanate (NaAlH₄) doped with nanostructured TiH₂ [40]. These studies demonstrate the possibility to meet the criteria for potential hydrogen storage materials for mobile applications, enhancing the kinetics without affecting the hydrogen capacity.

Therefore, this paper describes the synthesis, structural changes, thermal analysis and rehydrogenation ability of NaMgH₃, using diverse characterization methods such as ex-situ and in-situ X-ray Diffraction (XRD), Differential Scanning Calorimetry (DSC), and Thermogravimetric Analysis (TGA).

2. Materials and Methods

Powders of MgH₂ (95% pure hydride phase and 5% Mg; Sigma-Aldrich Inc.), NaH (95% pure; Sigma-Aldrich Inc.) were combined to obtain the perovskite-type NaMgH₃ ternary hydride. Powder mixtures were placed in a 250 mL stainless steel vial with 10 mm diameter balls (stainless steel) with a ball to sample mass ratio of 70:1. Mixtures were mechanically milled in a planetary ball mill instrument (Planetary Ball Mill PM400, Retsch, Birmingham, UK) in Ar for 4, 10 and 30 h (in total) at 400 rpm. To avoid dehydrogenation of the samples due to overheating during milling, periods of 5 min of milling and 5 min' rest time were established. As-prepared samples were unloaded inside an argon-filled glove box, placed in a dome-shaped sample holder, and then transferred to the ex-situ XRD with a D8 Advance diffractometer, Bruker, Birmingham, UK using Cu K α (0.154 nm) radiation, controlled by Diffract software (4.0 version) for analysis. In-Situ (XRD) measurements using an Anton Paar XRK 900 reactor, Bruker, Birmingham, UK chamber were performed to investigate the structural changes. The patterns were collected from 30 to 430 °C in 3 bar He, flowing at 100 mL/min for dehydrogenation, and 10 bar H₂ for rehydrogenation. Samples were enclosed in a boron nitride (BN) sample holder heated at a rate of 2 °C/min using a $5 \leq 2\theta \text{ (}^\circ\text{)} \leq 90$ range for phase determination. EVA software (equipped with PDF—2 database) [41] was used to analyze ex/in-situ diffractions. TOPAS Academic Software (4.0 version) [42] helped with the Pseudo-Rietveld Refinement and the references for data determination were obtained from the Inorganic Crystal Structure Database (ICSD) [43]. Background modeling was completed using Chebyshev function. Fitting of peak shapes were performed using the Pseudo-Voigt function. The lattice parameters were adjusted, following the atomic parameters. All points before 25 2 θ (°) were excluded from the refinement to obtain a more precise fitting.

Thermogravimetric analysis was executed using a TG 209, Netzsch, Birmingham, UK instrument operating at a heating rate of 2 °C/min, under 40 mL/min flowing argon. A 204 HP Phoenix DSC, Netzsch, Birmingham, UK instrument was used to collect the data information using a 3 bar constant pressure Ar flowing atmosphere at 100 mL/min and a temperature range of 25–430 °C at a heating rate of 2 °C/min. Thermal (DSC, TGA-MS) analysis were conducted inside an argon-filled glove box with purified argon of less than 5 ppm oxygen using alumina container covered with a lid.

3. Results and Discussion

3.1. Formation and Analysis of the NaMgH₃ Perovskite-Type Hydride

Ex-situ XRD diffractions of the mechanically milled NaH and MgH₂ for 2, 5 and 15 h are presented in Figure 1. After 2 h milling, peaks of the orthorhombic (space group Pnma) perovskite-type NaMgH₃ are observed, with the most intense peak located at ~32.8 (2 θ °). When milling for 5 h, the intensity of the main phase increases and more sharp peaks were evidenced. On further milling (15 h), there is evidence of sharper peaks related to the increased intensity of main NaMgH₃ phase. There are also unreacted peaks corresponding to MgO phase, probably formed during the milling process. No traces of remaining MgH₂ or unknown phases were detected after milling, and it is assumed that this effect was due to the relatively intensive milling conditions (400 rpm; ball to powder ratio 70:1). The

synthesis of the ternary hydride is completed after 2 h milling NaH and MgH₂, on further milling for 5 and 15 h increases the oxide fraction. This information indicates the facile synthesis of NaMgH₃ without the use of high-pressure techniques which is advantageous for scaling up (i.e., could be cost-effective).

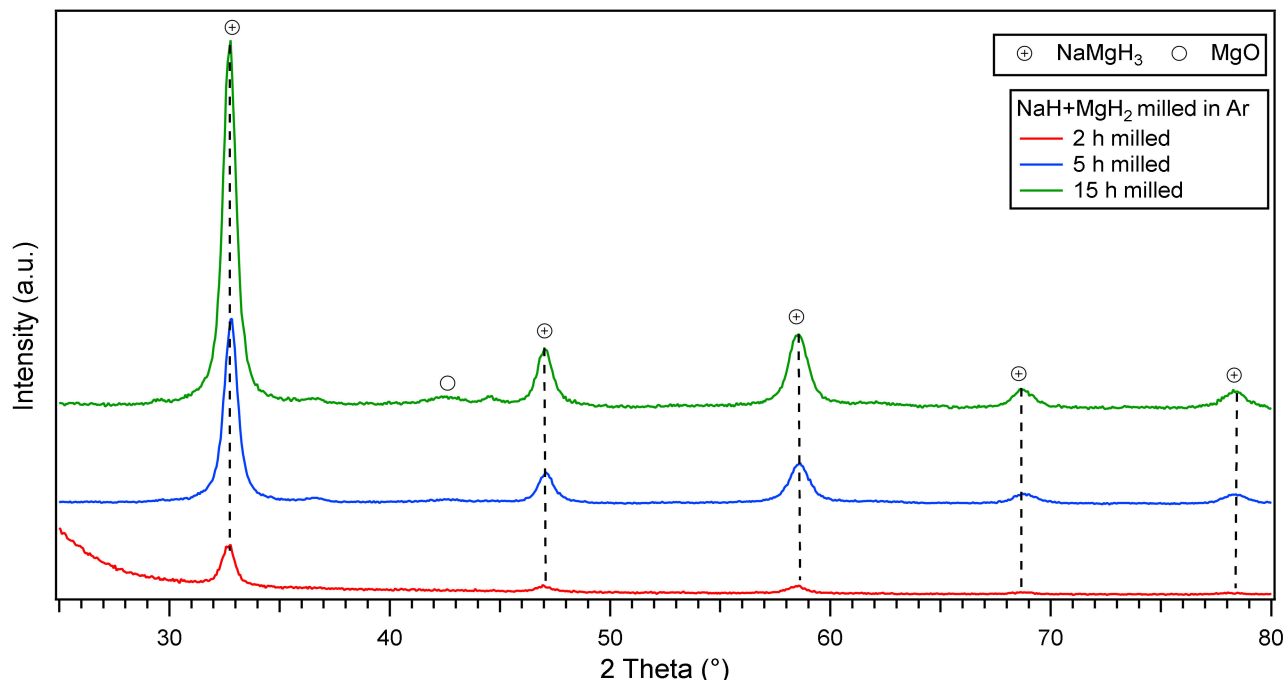


Figure 1. Ex-situ X-Ray Diffraction patterns of NaH and MgH₂ ball milled for 2, 5 and 15 h in argon showing main NaMgH₃ phase.

Rietveld refinement was used with TOPAS software to carry out more accurate structural research and to identify and quantify the primary phase of the milled NaMgH₃ hydride. Table 1 summarizes the evidence for the lattice parameters and cell volumes and compares previous reported data using a structural model based on Ikeda et al. [35] data collected from ICSD [43].

Table 1. Lattice parameters and cell volumes for the 2, 5 and 15 h milled NaMgH₃.

Atmosphere		NaMgH ₃ (This Work)			
Ar	Mill time (h)	lattice parameters (Å)			Cell Volume (Å ³)
		a	b	c	
	2	5.42 ± 0.01	7.76 ± 0.01	5.4 ± 0.01	230.19 ± 0.40
	5	5.49 ± 0.01	7.76 ± 0.01	5.43 ± 0.01	230.96 ± 0.60
	15	5.49 ± 0.01	7.76 ± 0.01	5.43 ± 0.01	231.28 ± 0.40
(Literature) [35]					
		Lattice Parameters (Å)			Cell Volume (Å ³)
		a	b	c	
		5.46 (2)	7.7 (4)	5.4 (2)	227.32 (4)

Lattice parameters obtained from the refinement show a slight increase when increasing milling time. Figure 2. illustrates the cell parameters (lattice and volume) of the NaMgH₃ hydride in function of the milling time experimentally calculated in this work. It is clear from the plot that there is a linear increase in the cell volume when milling for longer times; these reactions can be described by different factors, such as deformation caused by energy intense ball-milling or substitution reaction.

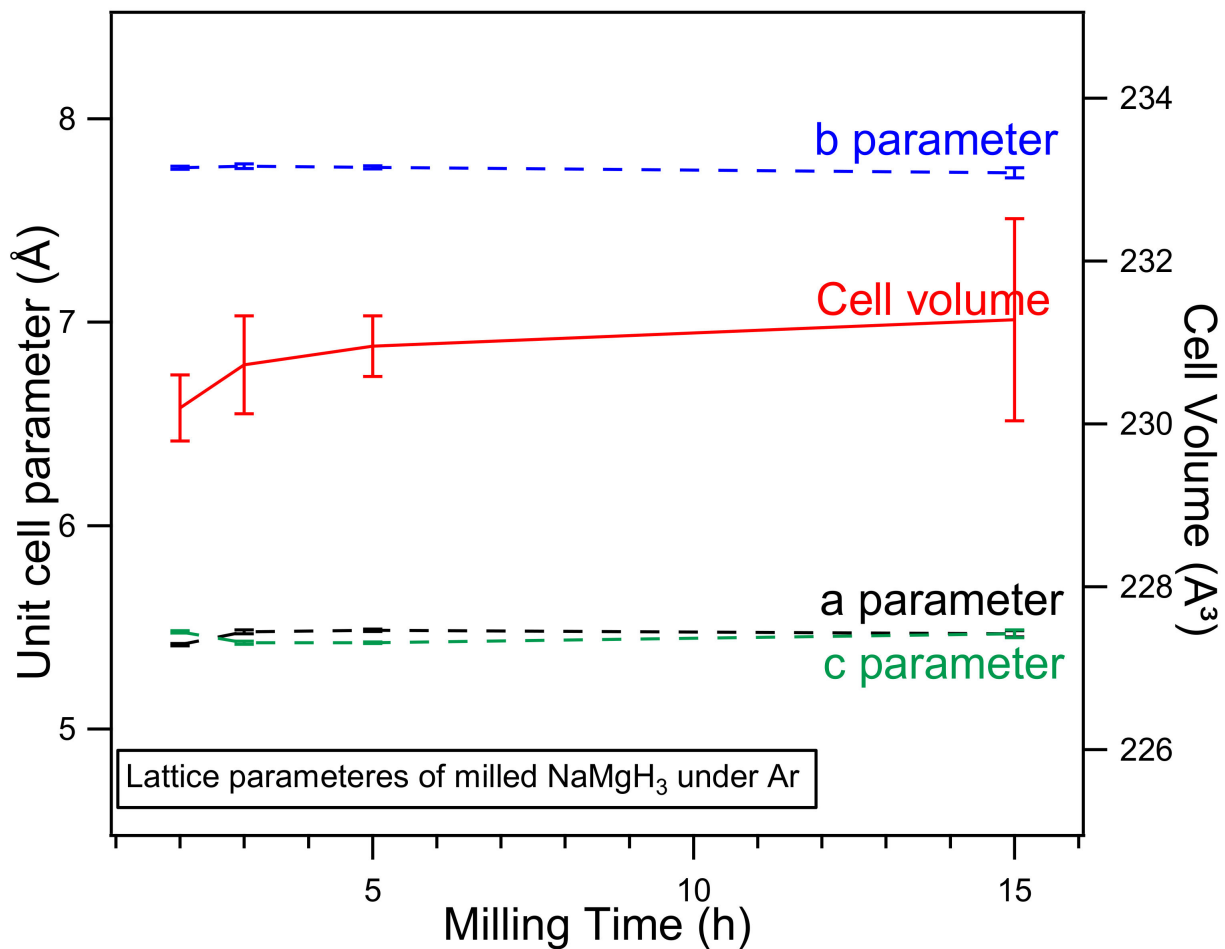


Figure 2. Unit cell parameters, a (black line), b (blue line), c (green line) (left) and Cell Volume parameters (red line) (right) of NaMgH₃ ternary hydride in function of the milling time. Error bars that are not displayed are smaller than data symbols.

3.2. Analysis of Hydrogen Storage Capacity

3.2.1. Thermal Analysis Performed by In-Situ XRD, DSC and TGA-MS

To analyze the dehydrogenating mechanisms, thermal changes and mass fluctuations of the ternary NaMgH₃, Thermal studies were performed using the DSC and TGA. Furthermore, to analyze the decomposition reactions and phase transitions in-situ XRD measurements were conducted. DSC, TGA-MS curves of 2, 5 and 15 h ball milled samples are presented in Figure 3.

NaMgH₃ (2 h Milled)

The dehydrogenation of the 2 h milled NaMgH₃ starts at ~300 °C; two consecutive endothermic reactions are evidenced from the DSC, with the maximum peak intensity at 370 °C and 383 °C, respectively. First reaction is linked to the dehydrogenation of the NaMgH₃ phase into NaH and Mg metal, while the second endotherm is associated with the transformation of NaH phase into Na metal; this corresponded to a total amount of hydrogen released of 5.8 wt.% up to 400 °C (TGA), 3.2 wt.% corresponds to the first release from 300 °C to 380 °C and 2.6 wt.% is related to the second release between 380 °C and 400 °C.

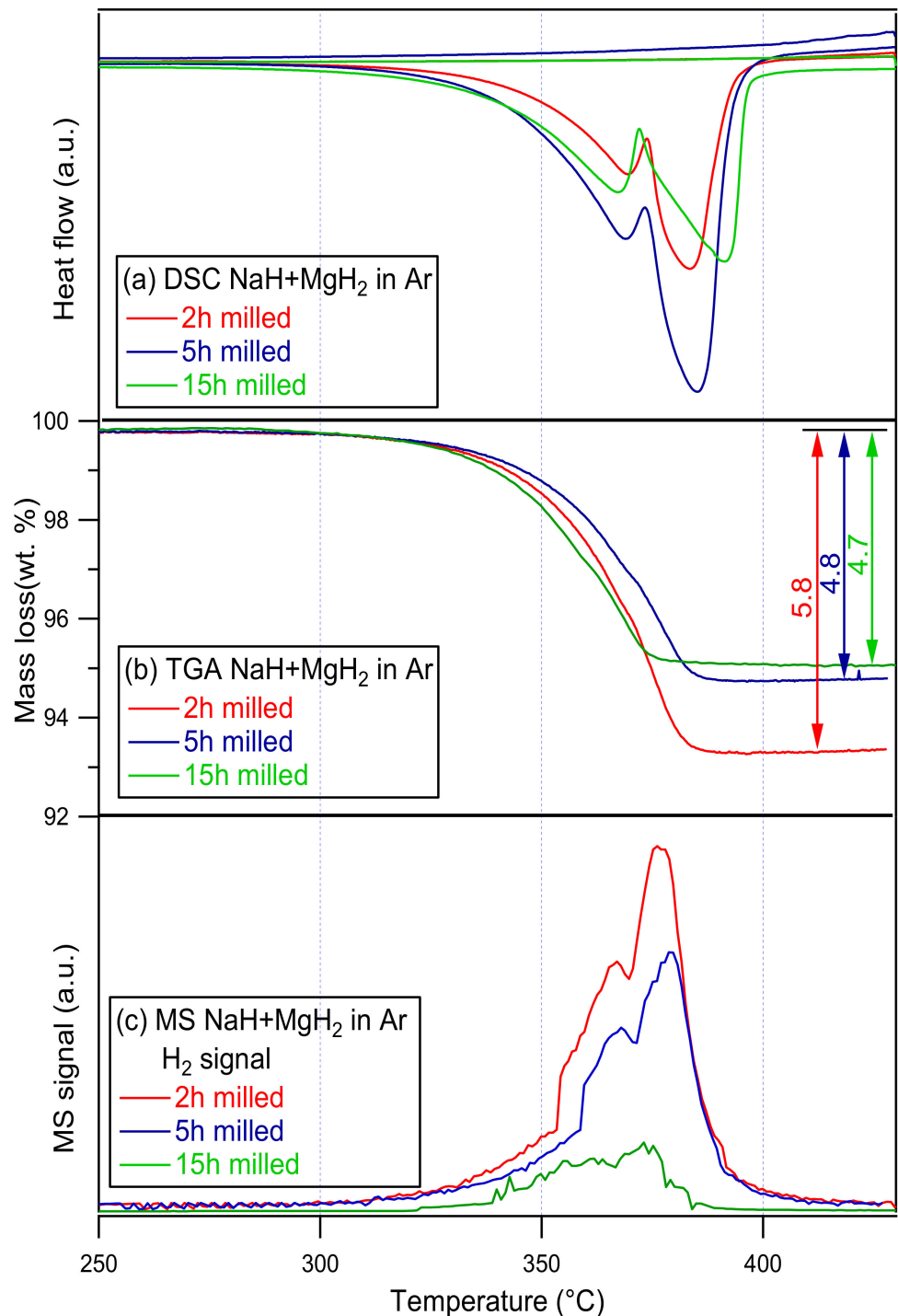


Figure 3. (a) DSC- (b) TG- (c) MS traces of 2, 5, 15 h milled NaMgH₃ samples. Measurements were conducted at a 2 °C/min heating rate from 30 °C to 430 °C under 3 bar Ar flowing at 100 mL/min (DSC), and 1 bar Ar flowing at 40 mL/min (TGA-MS).

The in-situ XRD of the 2 h milled NaMgH₃ sample is shown in Figure 4. From there it is evident that at 30 °C only diffractions of single phase NaMgH₃ were identified. Heating up to 330 °C, shows traces of NaH and Mg showing that the decomposition of the main NaMgH₃ has started. At 350 °C, more intense peaks of NaH and Mg are evidenced, along with some MgO diffractions. When heating to 400 °C only Mg metal diffractions alongside with MgO were observed. No evidence of Na was detected as would have been predicted

from the dehydrogenation of NaH. Nonetheless, it is thought that Na diffractions are present in the sample but have been oxidized as a result of a leak in the Anton Par cell used to do the measurements, causing the oxidation of Na metal and therefore preventing its detection.

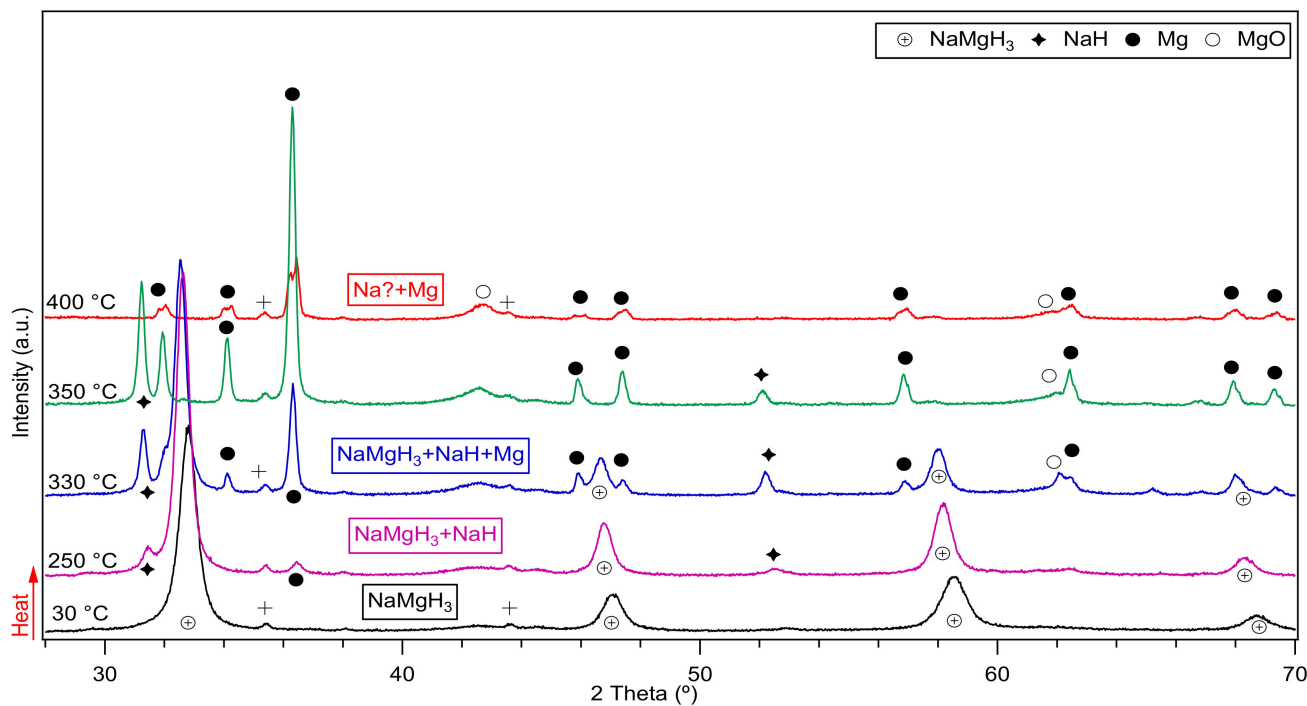
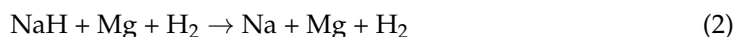
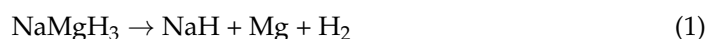


Figure 4. Decomposition reactions observed after in-Situ XRD measurements of the 2 h ball milled NaMgH₃ performed from 30 °C to 400 °C under 3 bar flowing He. The symbol + in the plot refers to traces related to the sample holder.

In order to confirm this assumption, the 2 h milled decomposed sample was taken to an argon filled glove box and hand mixed, then placed in a dome-shaped sample holder to perform ex-situ XRD measurements, diffractions related to Na, Mg and some traces of MgO phases were observed. Thus, confirming the presence of Na metal in the decomposed sample.

The decomposition reactions obtained from the measurements imply a two-step dehydrogenation process, as shown in Equations (1) and (2). Results agree with previous reported studies [20,24,35]. It is important to highlight that the equations below are not chemical equations, but a symbolic scheme of phase transitions observed during dehydrogenation of the NaMgH₃ ternary hydride.



NaMgH₃ (5 h Milled)

The DSC measurements of the 5 h milled NaMgH₃ hydride illustrate two endothermic curves, first for the NaMgH₃ decomposition into NaH and Mg peaking at 369 °C, and second for the NaH decomposition into Na releasing hydrogen and remaining magnesium peaking at 385 °C. A total of 4.8 wt.% of H₂ released up to 400 °C is shown by the TGA. Minor decrease (around 1 °C) is detected in temperature in comparison to the 2 h milled NaMgH₃.

In-situ XRD diffractions for the 5 h milled sample are shown in Figure 5. On heating from 30 °C to 300 °C, main NaMgH₃ phase is observed and small diffractions of NaH and

Mg were detected. At 330 °C, reflections of NaH and Mg become more intense showing decomposition of the main NaMgH₃ phase that is still present but less intense. When heating up to 350 °C, NaMgH₃ diffractions disappear, showing complete decomposition of the main phase and the only remaining phases observed correspond to crystalline Mg along with some reflections related to Mg oxide. On heating to 400 °C, same Mg and MgO phases were detected, as previously mentioned in the 2 h milled sample, no traces of Na metal were observed after 330 °C. Therefore, Ex-situ XRD measurements were conducted on the dehydrogenated sample to investigate this effect, and it was revealed that Na was present in the sample, but the instrument was not able to detect it due to an oxidation layer that formed on the surface.

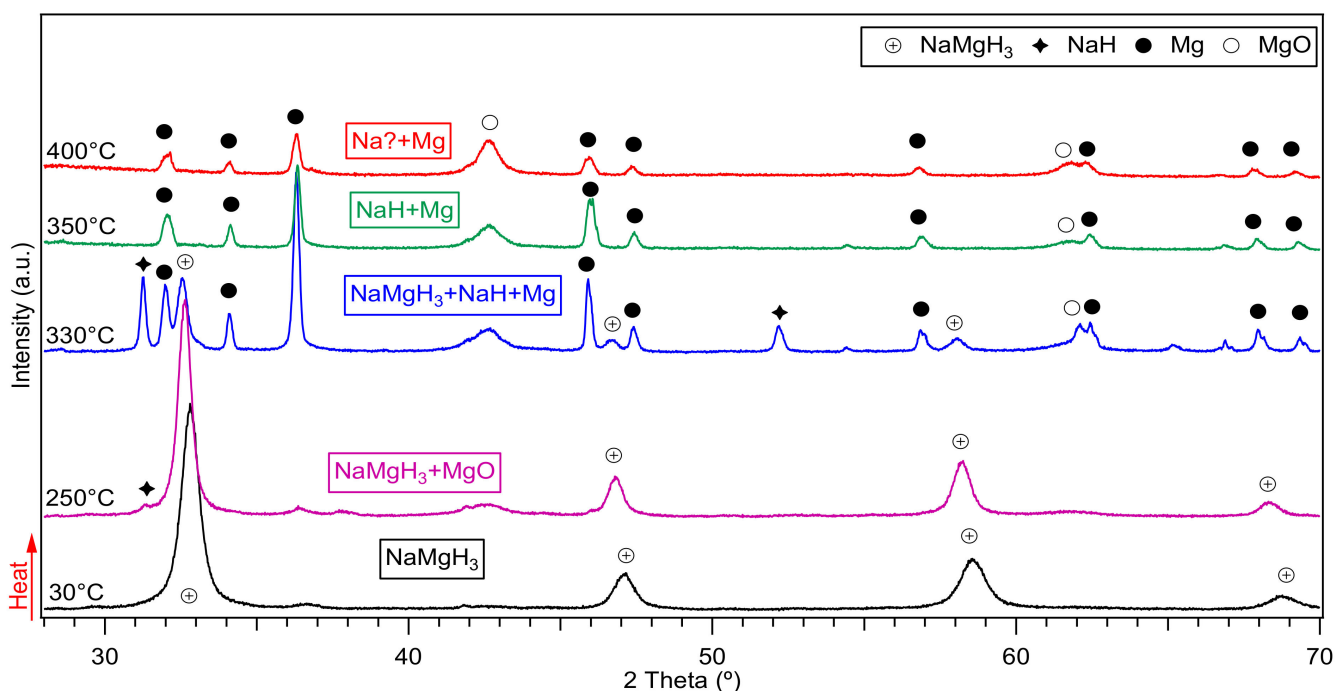


Figure 5. Dehydrogenation reactions shown by in-Situ XRD of the 5 h milled NaMgH₃ under 3 bar flowing He at 100 mL/min. Measurements taken from 30 °C to 400 °C.

The same two-step decomposition reactions as described in Equations (1) and (2), were observed in the 5 h milled NaMgH₃.

NaMgH₃ (15 h Milled)

For the 15 h milled NaMgH₃, DSC curves showed dehydrogenation proceeds in two steps: first endothermic peak at 367 °C, and second endothermic peak at 391 °C. No exothermic reactions were detected. Decomposition of NaMgH₃ into NaH and Mg is shown in the first curve, and the dehydrogenation of NaH into Na metal alongside with Mg is attributed to the second endotherm. The total amount of H₂ released detected from the TGA was 4.7 wt.%, from 278 to 400 °C.

In-situ diffraction patterns of the 15 h milled sample are shown in Figure 6. On heating from 30 °C to 250 °C, NaMgH₃ patterns were observed, in addition to some MgO peaks. On heating up to 330 °C, two new phases (NaH and Mg) attributed to the decomposition of the main phase were observed. Remaining traces of NaMgH₃ were detected decreasing in intensity with heating. At 350 °C, NaMgH₃ has completely decomposed, as no diffractions were observed. Diffractions of Mg and MgO were detected with increased intensity. On heating up to 400 °C, only traces of Mg were identified, along with diffractions of MgO.

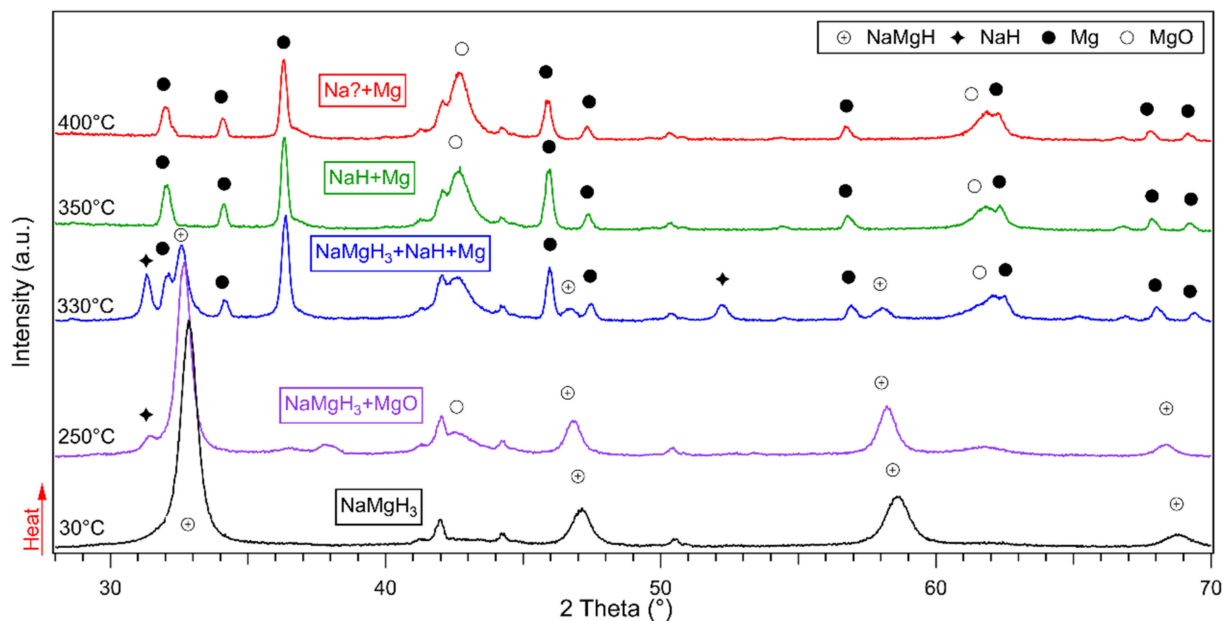


Figure 6. In-situ XRD diffractions taken from 30 to 400 °C of 15 h ball milled NaMgH₃ showing the dehydrogenation reactions under 3 bar flowing He.

Again, as in previous studied milled samples (2 h and 5 h) no peaks of NaH or Na metal were noticed. The nonappearance of Na diffractions after NaH dehydrogenation might be clarified by the increased intensity of the oxides peaks upon heating. After dehydrogenation, the sample was analyzed by ex-situ XRD to examine the decomposition products. From the analysis, peaks related to magnesium, sodium, and magnesium oxide were observed.

Measurements performed suggest a two-step dehydrogenation reactions (Equations (1) and (2)).

Summary of the experimentally collected results in this work for the DSC and TGA measurements (Figure 3) are presented in Table 2.

Table 2. Desorption temperatures (onset, peak 1, 2 and end) and hydrogen released from milled NaMgH₃ samples.

Atmosphere	M. Time (h)	DSC			TGA	
		T _{on} (°C)	T _{p1} (°C)	T _{p2} (°C)	T _{end} (°C)	wt (%) H ₂
Ar	2	287	370	383	408	5.8
	5	286	369	385	407	4.8
	15	278	367	391	409	4.7
Literature [14]	20		391	436		5.8

3.3. Rehydrogenation (In-Situ XRD)

After complete dehydrogenation of the 2, 5 and 15 h ball milled NaH and MgH₂ samples into crystalline Na and Mg, samples were exposed to heating under a 10 bar hydrogen atmosphere flowing at 100 mL/min at a heating rate of 2 °C/min with patterns taken isothermally from room temperature (~30 °C) to 400 °C, to investigate if NaMgH₃ main phase can be reversibly formed.

Results of the in-situ XRD measurements are plotted in Figure 7. Only one plot for the 5 h milled sample decomposed and reversibly formed is presented in this work, as the rehydrogenation on the 2 h and 15 h proceeds in the same way. Therefore, the author considered redundant to plot 3 figures with same information.

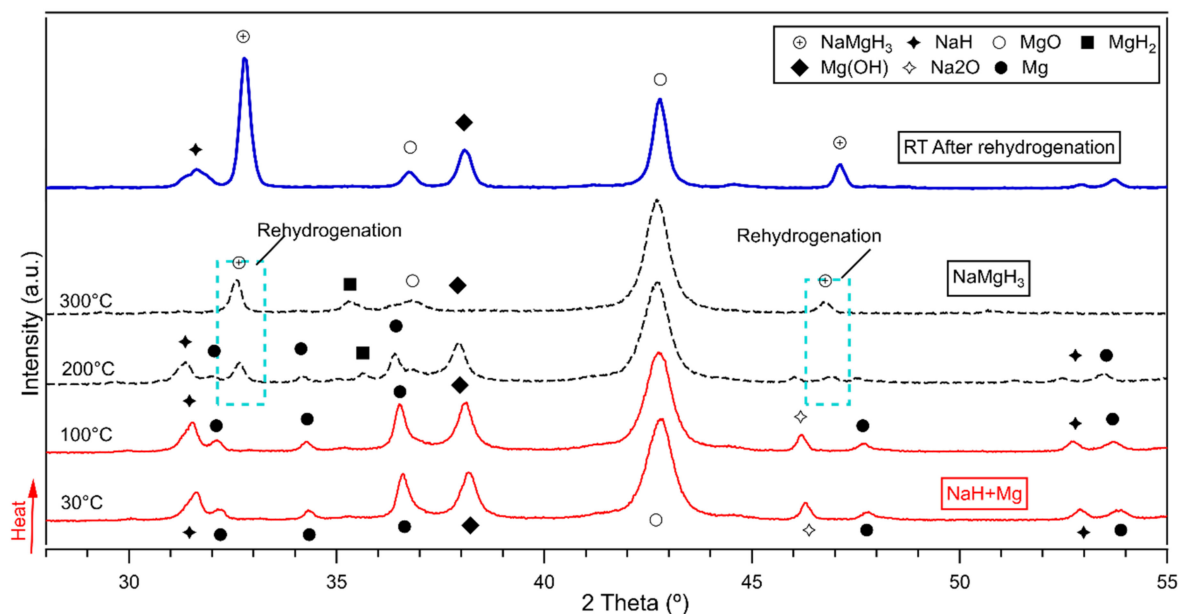


Figure 7. In-situ XRD of the 5 h milled NaMgH_3 showing rehydrogenation under 10 bar H_2 flowing at (100 mL/min) after decomposition. Measurements taken from 30 °C to 400 °C. Dashed (black line) shows rehydrogenation. (Blue thick line) shows ex-situ XRD after rehydrogenation.

Figure 7 illustrates the in-situ XRD diffractions of the formed NaMgH_3 phase after 5 h milling in Ar. On heating the decomposed sample from room temperature to 150 °C were identified diffraction patterns of NaH, Mg and Na oxide and Mg oxide. On further heating to 200 °C small diffractions related to the NaMgH_3 phase were detected, along with NaH, Mg, MgH_2 and sodium and magnesium oxides. At 300 °C, there are still small traces of MgH_2 and oxides, NaMgH_3 peaks become more intense with increasing heating up to 400 °C. This indicates that decomposed sample had been successfully rehydrogenated from Na and Mg. After rehydrogenation, ex-situ XRD measurements were performed, and Rietveld refinement was carried out to evaluate the phase fraction of the ternary hydride and other phases. From the refinement it is observed that rehydrogenated sample contains around 27 wt.% of NaMgH_3 phase, ~6 wt.% of NaH and the remaining products correspond to oxides.

NaMgH_3 were reversibly hydrogenated from Na and Mg phases as presented in Figure 7. These results show that NaMgH_3 can be easily formed and rehydrogenated from milling NaH and MgH_2 under relatively mild conditions (i.e., low pressure) which is advantageous for scaling up. Moreover, it is important to highlight that this work shows improved results in comparison to those reported from other studies.

4. Conclusions

NaMgH_3 perovskite-type hydride was synthesized by reactive milling under an inert (Ar) atmosphere and pressure. The synthesis of the ternary hydride was completed after only 2 h milling of Na and Mg hydrides, and further milling for 5 and 15 h increased the oxide fraction which reduced the hydrogen capacity. Dehydrogenation reactions were investigated experimentally. It was found that milled hydrides follow two-step decomposition, $\text{NaMgH}_3 \rightarrow \text{NaH} + \text{Mg} + \text{H}_2$ and $\text{NaH} + \text{Mg} + \text{H}_2 \rightarrow \text{Na} + \text{Mg} + \text{H}_2$. A significant increase in cell volume and lattice parameters is observed when milling is increased. The largest amount of H_2 release was observed in the two-hour milled NaMgH_3 sample, where 5.8 wt.% of H_2 was released from 287 to 408 °C. However, the lowest dehydrogenation peak temperature was detected at 367 °C for the 15 h milled NaMgH_3 . Milled NaMgH_3 samples for 2, 5 and 15 h were reversibly formed under 10 bar H_2 at 200 °C from the decomposed sodium and magnesium metals.

Author Contributions: Conceptualization, L.C. and D.B.; methodology, L.C. and A.B.; validation, L.C., M.M., L.R. and A.B.; formal analysis, L.C., M.M. and A.B.; investigation, L.C., M.M., A.B. and L.R.; writing—original draft preparation, L.C.; writing—review and editing, M.M., L.R. and A.B.; visualization, L.C., L.R. and A.B.; supervision, D.B. All authors have read and agreed to the published version of the manuscript.

Funding: This research was funded by Technical University of Ambato, Research and Development Directorate, Research Project ID PFICM23 “Análisis de la capacidad de generación de Hidrógeno como energía no contaminante mediante fuentes de energía renovables fotovoltaica y eólica”.

Institutional Review Board Statement: Not applicable.

Informed Consent Statement: Not applicable.

Data Availability Statement: The data presented in this study are available on request from the corresponding author.

Conflicts of Interest: The authors declare no conflict of interest.

References

1. Sherif, S.A.; Goswami, D.Y.; Stefanakos, E.K.; Steinfeld, A. *Handbook of Hydrogen Energy*; CRC Press: Boca Raton, FL, USA, 2014; pp. 17–18.
2. Lin, R.H.; Zhao, Y.Y.; Wu, B.D. Toward a hydrogen society: Hydrogen and smart grid integration. *Int. J. Hydrogen Energy* **2020**, *45*, 20164–20175. [[CrossRef](#)]
3. Abe, J.O.; Popoola, A.P.I.; Ajenifuja, E.; Popoola, O.M. Hydrogen energy, economy and storage: Review and recommendation. *Int. J. Hydrogen Energy* **2019**, *44*, 15072–15086. [[CrossRef](#)]
4. Nazir, H.; Louis, C.; Jose, S.; Prakash, J.; Muthuswamy, N.; Buan, M.E.M.; Flox, C.; Chavan, S.; Shi, X.; Kauranen, P.; et al. Is the H₂ economy realizable in the foreseeable future? Part I: H₂ production methods. *Int. J. Hydrogen Energy* **2020**, *45*, 13777–13788. [[CrossRef](#)]
5. Fonseca, J.D.; Camargo, M.; Commenge, J.M.; Falk, L.; Gil, I.D. Trends in design of distributed energy systems using hydrogen as energy vector: A systematic literature review. *Int. J. Hydrogen Energy* **2019**, *44*, 9486–9504. [[CrossRef](#)]
6. Zhang, F.; Zhao, P.; Niu, M.; Maddy, J. The survey of key technologies in hydrogen energy storage. *Int. J. Hydrogen Energy* **2016**, *41*, 14535–14552. [[CrossRef](#)]
7. Dincer, I.; Acar, C. Review and evaluation of hydrogen production methods for better sustainability. *Int. J. Hydrogen Energy* **2015**, *40*, 11094–11111. [[CrossRef](#)]
8. Rusman, N.A.A.; Dahari, M. A review on the current progress of metal hydrides material for solid-state hydrogen storage applications. *Int. J. Hydrogen Energy* **2016**, *41*, 12108–12126. [[CrossRef](#)]
9. Barthelemy, H.; Weber, M.; Barbier, F. Hydrogen storage: Recent improvements and industrial perspectives. *Int. J. Hydrogen Energy* **2017**, *42*, 7254–7262. [[CrossRef](#)]
10. Andersson, J.; Grönkvist, S. Large-scale storage of hydrogen. *Int. J. Hydrogen Energy* **2019**, *44*, 11901–11919. [[CrossRef](#)]
11. Bouamrane, A.; Soulié, J.P.; Bastide, J.P. Standard enthalpies of formation of KCaH_{3-x}F_x with x = 1, 1.5, 2, 2.5. *Thermochim. Acta* **2001**, *375*, 81–84. [[CrossRef](#)]
12. Bouhadda, Y.; Boudouma, Y.; Fennineche, N.E.; Bentabet, A. Ab initio calculations study of the electronic, optical and thermodynamic properties of NaMgH₃, for hydrogen storage. *J. Phys. Chem. Solids* **2010**, *71*, 1264–1268. [[CrossRef](#)]
13. Bouhadda, Y.; Bououdina, M.; Fennineche, N.; Boudouma, Y. Elastic properties of perovskite-type hydride NaMgH₃ for hydrogen storage. *Int. J. Hydrogen Energy* **2013**, *38*, 1484–1489. [[CrossRef](#)]
14. Ikeda, K.; Kogure, Y.; Nakamori, Y.; Orimo, S. Formation region and hydrogen storage abilities of perovskite-type hydrides. *Prog. Solid State Chem.* **2007**, *35*, 329–337. [[CrossRef](#)]
15. Zaluski, L.; Zaluska, A.; Ström-Olsen, J.O. Nanocrystalline metal hydrides. *J. Alloys Compd.* **1997**, *253–254*, 70–79. [[CrossRef](#)]
16. Zaluska, A.; Zaluski, L.; Ström-Olsen, J.O. Structure, catalysis and atomic reactions on the nano-scale: A systematic approach to metal hydrides for hydrogen storage. *Appl. Phys. A* **2001**, *72*, 157–165. [[CrossRef](#)]
17. Amica, G. *Preparación, Estudio y Optimización de Amiduros de Litio y Magnesio para Almacenamiento de Hidrógeno*; Universidad Nacional de Cuyo: Mendoza, Argentina, 2018.
18. Wu, H.; Zhou, W.; Udovic, T.J.; Rush, J.J.; Yildirim, T. Crystal chemistry of perovskite-type hydride NaMgH₃: Implications for hydrogen storage. *Chem. Mater.* **2008**, *20*, 2335–2342. [[CrossRef](#)]
19. Rönnebro, E.; Noréus, D.; Kadir, K.; Reiser, A.; Bogdanovic, B. Investigation of the perovskite related structures of NaMgH₃, NaMgF₃ and Na₃AlH₆. *J. Alloys Compd.* **2000**, *299*, 101–106. [[CrossRef](#)]
20. Reardon, H.; Mazur, N.; Gregory, D.H. Facile synthesis of nanosized sodium magnesium hydride, NaMgH₃. *Prog. Nat. Sci. Mater. Int.* **2013**, *23*, 343–350. [[CrossRef](#)]
21. Ikeda, K.; Kato, S.; Shinzato, Y.; Okuda, N.; Nakamori, Y.; Kitano, A.; Yukawa, H.; Morinaga, M.; Orimo, S. Thermodynamical stability and electronic structure of a perovskite-type hydride, NaMgH₃. *J. Alloys Compd.* **2007**, *446–447*, 162–165. [[CrossRef](#)]

22. Fornari, M.; Subedi, A.; Singh, D.J. Structure and dynamics of perovskite hydrides $AMgH_3$ ($A = Na, K, Rb$) in relation to the corresponding fluorides: A first-principles study. *Phys. Rev. B Condens. Matter Mater. Phys.* **2007**, *76*, 214118. [CrossRef]
23. Li, D.; Zhang, T.; Yang, S.; Tao, Z.; Chen, J. Ab initio investigation of structures, electronic and thermodynamic properties for Li–Mg–H ternary system. *J. Alloys Compd.* **2011**, *509*, 8228–8234. [CrossRef]
24. Pottmaier, D.; Pinatel, E.R.; Vitillo, J.G.; Garroni, S.; Orlova, M.; Baró, M.D.; Vaughan, G.B.M.; Fichtner, M.; Lohstroh, W.; Baricco, M. Structure and thermodynamic properties of the $NaMgH_3$ perovskite: A comprehensive study. *Chem. Mater.* **2011**, *23*, 2317–2326. [CrossRef]
25. Reshak, A.H. $NaMgH_3$ a perovskite-type hydride as advanced hydrogen storage systems: Electronic structure features. *Int. J. Hydrogen Energy* **2015**, *40*, 16383–16390. [CrossRef]
26. Tao, S.; Wang, Z.M.; Li, J.J.; Deng, J.Q.; Zhou, H.; Yao, Q.R. Improved Dehydrogenating Properties of $NaMgH_3$ Perovskite Hydride by Addition of Graphitic Carbon Nitride. *Mater. Sci. Forum* **2016**, *852*, 502–508. [CrossRef]
27. Komiyama, K.; Morisaku, N.; Rong, R.; Takahashi, Y.; Shinzato, Y.; Yukawa, H.; Morinaga, M. Synthesis and decomposition of perovskite-type hydrides, $MMgH_3$ ($M = Na, K, Rb$). *J. Alloys Compd.* **2008**, *453*, 157–160. [CrossRef]
28. Sheppard, D.A.; Paskevicius, M.; Buckley, C.E. Thermodynamics of hydrogen desorption from $NaMgH_3$ and its application as a solar heat storage medium. *Chem. Mater.* **2011**, *23*, 4298–4300. [CrossRef]
29. Klaveness, A.; Swang, O.; Fjellvag, H. Formation enthalpies of $NaMgH_3$ and $KMgH_3$: A computational study. *Europhys. Lett.* **2006**, *76*, 285. [CrossRef]
30. Hydrogen and Fuel Cell Technologies Office. DOE Technical Targets for Onboard Hydrogen Storage for Light-Duty Vehicles. Available online: <https://www.energy.gov/eere/fuelcells/doe-technical-targets-onboard-hydrogen-storage-light-duty-vehicles> (accessed on 15 December 2021).
31. Wang, Z.; Tao, S.; Deng, J.; Zhou, H.; Yao, Q. Significant improvement in the dehydrogenating properties of perovskite hydrides, $NaMgH_3$, by doping with K_2TiF_6 . *Int. J. Hydrogen Energy* **2017**, *42*, 8554–8559. [CrossRef]
32. Chaudhary, A.L.; Paskevicius, M.; Sheppard, D.A.; Buckley, C.E. Thermodynamic destabilisation of MgH_2 and $NaMgH_3$ using Group IV elements Si, Ge or Sn. *J. Alloys Compd.* **2015**, *623*, 109–116. [CrossRef]
33. Martínez-Coronado, R.; Sánchez-Benítez, J.; Retuerto, M.; Fernández-Díaz, M.T.; Alonso, J.A. High-pressure synthesis of $Na_{1-x}Li_xMgH_3$ perovskite hydrides. *J. Alloys Compd.* **2012**, *522*, 101–105. [CrossRef]
34. Ikeda, K.; Nakamori, Y.; Orimo, S. Formation ability of the perovskite-type structure in $Li_xNa_{1-x}MgH_3$ ($x = 0, 0.5$ and 1.0). *Acta Mater.* **2005**, *53*, 3453–3457. [CrossRef]
35. Ikeda, K.; Kogure, Y.; Nakamori, Y.; Orimo, S. Reversible hydriding and dehydrogenating reactions of perovskite-type hydride $NaMgH_3$. *Scr. Mater.* **2005**, *53*, 319–322. [CrossRef]
36. Tao, S.; Wang, Z.-m.; Wan, Z.-z.; Deng, J.-q.; Zhou, H.; Yao, Q. Enhancing the dehydrogenating properties of perovskite-type $NaMgH_3$ by introducing potassium as dopant. *Int. J. Hydrogen Energy* **2017**, *42*, 3716–3722. [CrossRef]
37. Hang, Z.; Hu, Z.; Xiao, X.; Jiang, R.; Zhang, M. Enhancing Hydrogen Storage Kinetics and Cycling Properties of $NaMgH_3$ by 2D Transition Metal Carbide $MXene Ti_3C_2$. *Processes* **2021**, *9*, 1690. [CrossRef]
38. Zhang, X.; Liu, Y.; Ren, Z.; Zhang, X.; Hu, J.; Huang, Z.; Lu, Y.; Gao, M.; Pan, H. Realizing 6.7 wt% reversible storage of hydrogen at ambient temperature with non-confined ultrafine magnesium hydrides. *Energy Environ. Sci.* **2021**, *14*, 2302–2313. [CrossRef]
39. Zhang, X.; Zhang, L.; Zhang, W.; Ren, Z.; Huang, Z.; Hu, J.; Gao, M.; Pan, H.; Liu, Y. Nano-synergy enables highly reversible storage of 9.2 wt% hydrogen at mild conditions with lithium borohydride. *Nano Energy* **2021**, *83*, 105839. [CrossRef]
40. Ren, Z.; Zhang, X.; Li, H.-W.; Huang, Z.; Hu, J.; Gao, M.; Pan, H.; Liu, Y. Titanium Hydride Nanoplates Enable 5 wt% of Reversible Hydrogen Storage by Sodium Alanate below 80 °C. *Research* **2021**, *2021*, 9819176. [CrossRef]
41. Bruker. Bruker DIFFRAC.SUITE EVA—XRD Software. Available online: <https://www.bruker.com/products/x-ray-diffraction-and-elemental-analysis/x-ray-diffraction/xrd-software/eva.html> (accessed on 18 October 2020).
42. Bruker. Bruker DIFFRAC.SUITE TOPAS—XRD Software, X-ray Diffraction—XRD Software. Available online: <https://www.bruker.com/products/x-ray-diffraction-and-elemental-analysis/x-ray-diffraction/xrd-software/topas.html> (accessed on 18 October 2020).
43. ICSD Inorganic Chemical Database Service. Available online: <http://icsd.cds.rsc.org/search/basic.xhtml?sessionid=82761CD648F766CC9CA76BDA84933E21?cdsrd=3> (accessed on 18 October 2020).